Cation Substitution in Defect Thiospinels: Structural and Magnetic Properties of $GaV_{4-x}Mo_xS_8$ ($0 \leq x \leq 4$)

Anthony V. Powell,*,† Andrew McDowall,† Iwona Szkoda,† Kevin S. Knight,‡ Brendan J. Kennedy,§ and Thomas Vogt||

Department of Chemistry, Heriot-Watt University, Edinburgh EH14 4AS, U.K., ISIS Facility, Rutherford Appleton Laboratory, Didcot, Oxfordshire OX11 0QX, U.K., School of Chemistry, F11, The University of Sydney, Sydney, New South Wales 2006, Australia, and NanoCenter and Department of Chemistry and Biochemistry, University of South Carolina, Columbia, South Carolina 29208

Received May 18, 2007. Revised Manuscript Received July 10, 2007

A new family of nonstoichiometric materials, $GaV_{4-x}Mo_xS_8$ ($0 \leq x \leq 4$), has been prepared and characterized by high-resolution neutron powder diffraction, laboratory and synchrotron X-ray powder diffraction, thermogravimetry, and SQUID magnetometery. All materials adopt a cubic ($F\bar{4}3m$) structure at ambient temperature. The end-member phases GaV_4S_8 and $GaMo_4S_8$ exhibit a distortion to rhombohedral ($R3m$) symmetry at low temperatures. High-resolution powder neutron diffraction reveals that the phase transition is incomplete and that both cubic and rhombohedral phases coexist below ca. 40 K. Magnetic susceptibility data indicate that at low temperatures, the end-member phases undergo a transition to a ferromagnetic state in which the metal−metal exchange interactions within cubic B_4S_4 clusters are predominantly antiferromagnetic in origin. At intermediate compositions ($1 \leq x \leq 3$) a cubic structure persists to 4 K, and materials remain paramagnetic to this temperature. The suppression of the rhombohedral distortion may be responsible for the absence of magnetic ordering observed in the nonstoichiometric members of the $GaV_{4-x}Mo_xS_8$ series.

Introduction

Many compounds of general formula AB_2S_4 adopt the spinel structure in which one-third of the cations occupy tetrahedral sites and the remainder are octahedrally coordinated. By contrast with transition-metal sulfides with NiAs-related structures, for which variations in stoichiometry give rise to a range of vacancy-ordered phases,[1,2] cation-deficiency is less common in the thiospinels: stable phases generally being confined to the stoichiometric composition. However, a small family of spinel-related materials exists in which 50% cation-deficiency associated with the A-site gives rise to a superstructure. Ternary phases of general formula $A_{0.5}B_2S_4$ ($\equiv AB_4S_8$) have been reported for A = Ga, Al, Ge, Fe−Ni, Zn and B = Mo, V, Nb, Ta, (Mo/Re).[3,4,5,6,7] The structure of these defective thiospinels consists of heterocubane-like $B_4X_4^{n+}$ units and AX_4^{n-} tetrahedra arranged in a similar manner to the ions in the rock-salt structure (Figure 1). Ordering of the cation vacancies over the tetrahedral A-sites lowers the symmetry of the ideal spinel structure ($Fd\bar{3}m$) to $F\bar{4}3m$. Furthermore, displacement of the octahedral B-site cations gives rise to B_4 clusters with short B−B distances.

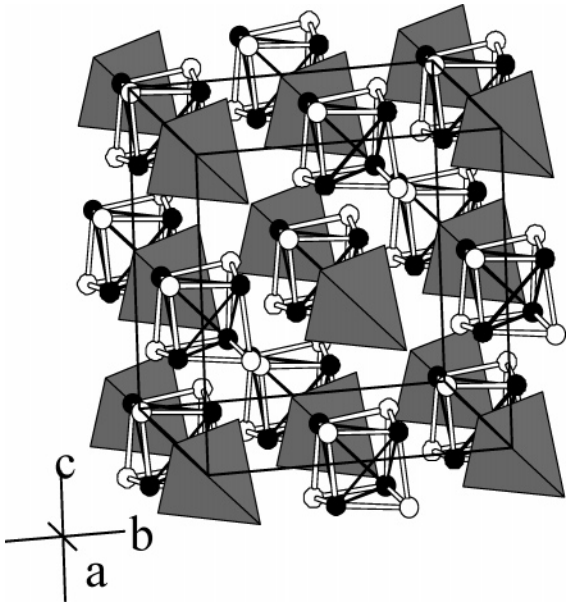

Figure 1. The defect thiospinel structure of GaV_4S_8. Vanadium atoms are shown as solid circles, sulfur atoms are shown by open circles, and GaS_4 tetrahedra are shaded. V−S bonds are shown as open lines, and solid lines denote the V−V interactions that define a V_4 cluster.

These materials are Mott insulators, in which electrical conduction occurs by hopping of electrons[8] between clusters separated by relatively large distances of ca. 4 Å. It has been

* Corresponding author fax: +44 (0)131 451 3180; e-mail: a.v.powell@hw.ac.uk.
† Heriot-Watt University.
‡ Rutherford Appleton Laboratory.
§ The University of Sydney.
|| University of South Carolina.

(1) Kjeshus, A.; Pearson, W. B. *Prog. Solid State Chem.* **1964**, *1*, 83.
(2) Vaqueiro, P.; Powell, A. V. *Chem. Mater.* **2000**, *12*, 2705.
(3) Barz, H. *Mater. Res. Bull.* **1973**, *8*, 983.
(4) Perrin, C.; Chevrel, R.; Sergent, M. *C. R. Acad. Sci. Paris* **1975**, *C280*, 949.
(5) Ben Yaichi, H.; Jegaden, J. C.; Potel, M.; Sergent, M.; Rastogi, A. K.; Tournier, R. *J. Less Common Met.* **1984**, *102*, 9.
(6) Perrin, C.; Chevrel, R.; Sergent, M. *J. Solid State Chem.* **1976**, *19*, 305.
(7) Johrendt, D. *Z. Anorg. Allg. Chem.* **1998**, *624*, 952.
(8) Sahoo, Y.; Rastogi, A. K. *J. Phys. Condens. Matter* **1993**, *5*, 5953.

10.1021/cm071354t CCC: $37.00
Published on Web 09/01/2007

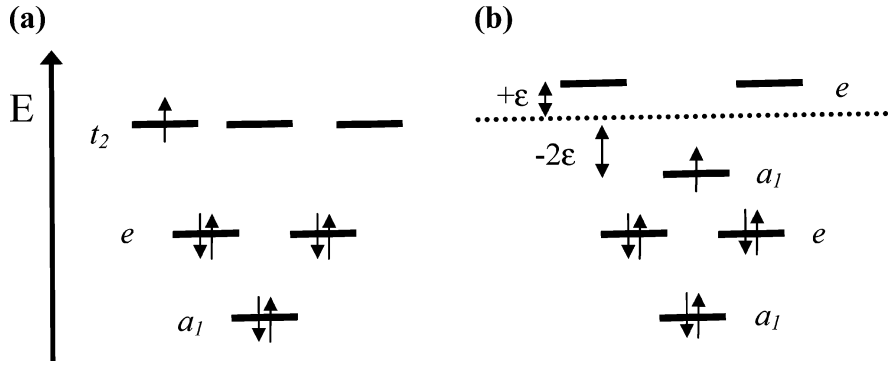

Figure 2. Molecular orbital scheme for metal-based orbitals of the B_4 cluster in AB_4S_8 (after Pocha et al.[11]): (a) a cluster of tetrahedral symmetry in the cubic structure and (b) a cluster of C_{3v} symmetry for a rhombohedral distortion with $\alpha < 60°$. The energies of the higher-lying *e* and a_1 orbitals are reversed for $\alpha > 60°$. The orbital filling refers to the composition GaV_4S_8.

suggested that GaV_4S_8 behaves as an electron glass at low temperatures,[9] while $GaNb_4S_8$ has recently been shown to undergo a pressure-induced transition to a superconducting state (T_c=4 K at 23 GPa).[10] The unpaired electrons associated with partially-filled cluster orbitals are effectively localized on the B_4 cluster, with the result that, at low temperatures, the materials may exhibit cooperative magnetic phenomena, the nature of which is dependent on the degree of cluster orbital filling. For example, the ternary phases $GaMo_4S_8$ and GaV_4S_8, exhibit weak ferromagnetism below T_c of 16 K[3] and 10 K,[11] respectively, while GeV_4S_8 is antiferromagnetic (T_N=15 K).[7,12] Anomalies observed at ca. 40 K in magnetic susceptibility data of $GaMo_4S_8$ and GaV_4S_8 have been assigned to structural transitions in the paramagnetic phase of these materials. Powder X-ray diffraction studies[13] of $GaMo_4S_8$ reveal a low-temperature transition to rhombohedral symmetry, involving a compression along the body diagonal of the cubic unit cell. Given the similarity of the magnetic susceptibility data, an analogous distortion has long been assumed to occur in GaV_4S_8, but Pocha et al.[11] recently suggested, on the basis of Rietveld refinement using medium resolution laboratory powder X-ray diffraction data, that while GaV_4S_8 also undergoes a cubic to rhombohedral transition at low temperature, the distortion is in the opposite sense to that in $GaMo_4S_8$, involving expansion along the body diagonal. However, peak splittings were poorly resolved, and significant features remained in the difference profiles. By considering the metal-based orbitals on the B_4 cluster (Figure 2), the opposing nature of the distortion in the vanadium and molybdenum phases was rationalized in terms of the differing crystal field stabilization energies.

In this work, we sought to explore the relationship between the structural distortion and the magnetic ordering phenomena by varying the electron count in the B_4 cluster, through progressive substitution of vanadium by molybdenum in the series $GaV_{4-x}Mo_xS_8$ ($0 \le x \le 4$). Each integral step in composition introduces one additional electron into the orbitals based on the B_4 cluster. The results demonstrate that in bulk samples the structural distortion is incomplete in the end-member phases and is suppressed completely in the non-stoichiometric materials, with the result that quaternary phases do not exhibit a magnetic ordering transition at low temperatures.

Experimental Section

Samples of $GaV_{4-x}Mo_xS_4$ ($0 \le x \le 4$) were synthesized by firing mixtures of the elements at elevated temperatures. Appropriate mixtures of molybdenum (Alfa 99.95%), vanadium (Aldrich, 99.5%), and sulfur (Aldrich, 99.9%) powders were ground in an agate mortar and then loaded into a silica tube, to which was added the required quantity of slivers of gallium (Alfa 99.99%) cut from an ingot. In all cases a small excess (5%) of molybdenum was required, in order to suppress the formation of Ga_2S_3 which otherwise formed: consequently reaction mixtures with Ga:V:Mo:S molar ratios of 1:(4-*x*):1.05*x*:8 were prepared in all cases. This need for a slight excess of molybdenum in the reaction mixture is in agreement with the findings of Shamrai et al.,[14] while we observed that a larger excess led to the formation of MoS_2. The silica tubes were evacuated to $\le 10^{-4}$ Torr before being sealed. All molybdenum-containing reaction mixtures were placed directly into a furnace at 1000 °C and held at this temperature for 24 h, prior to regrinding and refiring at 1000 °C for a further 72 h. GaV_4S_8 was prepared in an analogous fashion at a temperature of 800 °C.

All products were characterized by laboratory powder X-ray diffraction using a Philips PA2000 diffractometer operating with nickel-filtered Cu-K_α radiation. Data were collected in step-scan mode using a step-size of 0.02°(2θ) and a counting time of 5 s step^{-1}. The sulfur content was determined thermogravimetrically by oxidation in a flow of dry oxygen on a DuPont Instruments 951 Thermogravimetric Analyzer. Magnetic susceptibility measurements were made using a Quantum Design MPMS2 SQUID susceptometer. Samples were loaded into gelatin capsules at room temperature. Data were collected over the temperature range $2 \le T/K \le 300$ both after cooling the sample in zero-field (zfc) and after cooling in the measuring field (fc) of 1 kG. Data were corrected for the diamagnetism of the gelatin capsule and for intrinsic core diamagnetism. In addition, the magnetization at 5 K was measured for the end-member phases, $GaMo_4S_8$ and GaV_4S_8, as a function of applied field in the range 0.1−10 kG.

High-resolution time-of-flight powder neutron diffraction data for all materials were collected using the HRPD diffractometer at ISIS, Rutherford Appleton Laboratory, U.K. Data over the time-

(9) Rastogi, A. K.; Niazi, A. *Physica B (Amsterdam)* **1996**, *223 & 224*, 588.
(10) Pocha, R.; Johrendt, D.; Ni, B.; Abd-Elmeguid, M. M. *J. Am. Chem. Soc.* **2005**, *127*, 8732.
(11) Pocha, R.; Johrendt, D.; Pöttgen, R. *Chem. Mater.* **2000**, *12*, 2882.
(12) Müller, H.; Kockelman, W.; Johrendt, D. *Chem. Mater.* **2006**, *18*, 2174.
(13) Francois, M.; Lengauer, W.; Yvon, K.; Ben Yaich-Aerrache, H.; Gourgeon, P.; Potel, M.; Sergent, M. *Z. Kristallogr.* **1991**, *196*, 111.
(14) Shamrai, V. F.; Leitus, G. M. *Izv. Akad. Nauk. SSSR Met.* **1983**, *1*, 162.

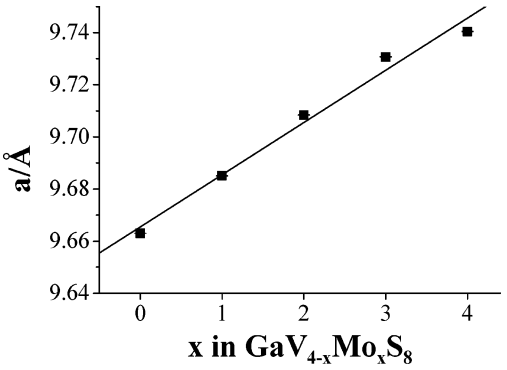

Figure 3. Compositional variation of the cubic lattice parameter of $GaV_{4-x}Mo_xS_8$ ($0 \le x \le 4$) determined at room temperature by laboratory powder X-ray diffraction data.

of-flight range 30−130 ms were collected on ca. 3 g of sample contained in flat-slab aluminum cans, with vanadium windows, mounted in a cryostat. Initial data manipulation and reduction were carried out using Genie spectrum manipulation software. Neutron diffraction data from the backscattering (2θ=168°) and 90° detector banks, corresponding to *d*-spacings in the range 0.7−2.3 Å and 1−3.2 Å, respectively, were summed, normalized, and used simultaneously in Rietveld refinement.

Owing to the small neutron scattering length of vanadium, complementary high-resolution synchrotron powder X-ray diffraction data were collected for GaV_4S_8. Data at 300 K and above were obtained at The Australian National Beamline Facility, BL-20, The Photon Factory, Tsukuba, Japan.[15] The sample was contained in a rotating 0.3 mm diameter glass capillary held in a furnace. Data were collected, using an incident wavelength of 0.99880 Å, in two image plates, each covering 40° in 2θ giving data with a step size of 0.01° over the angular range $3 \le 2\theta/° \le 83$. Data below 300 K were recorded with the X7A beamline at the NSLS, Brookhaven National Laboratory, U.S.A. The sample was again contained in a continuously rotating capillary held in a cryostat. Data were collected over the angular range $9 \le 2\theta/° \le 61$ in 0.01° steps, using a wavelength of 0.704468 Å. All Rietveld refinements were carried out using the GSAS package.[16]

Results and Discussion

Laboratory powder X-ray diffraction data for samples throughout the composition range $0 \le x \le 4$ can be indexed on a cubic unit cell with a lattice parameter similar to that reported by Pocha et al.[11] for the end-member (x=0) phase GaV_4S_8. The cubic lattice parameter shows an almost linear increase with increasing levels of molybdenum incorporation, suggesting formation of a solid solution across the whole range of composition (Figure 3).

Thermogravimetric analysis of GaV_4S_8 (Figure 4(a)) reveals a weight loss of 15.6% at 425 °C, associated with conversion to $Ga_2O_3 + V_4O_9$ (calculated, 16.7%), followed by a weight gain of 3.0% due to oxidation to V_2O_5 (calculated, 2.3%). For the other end-member, $GaMo_4S_8$, a weight loss of 5.71% at 450 °C (Figure 4(b)) arising from conversion to $Ga_2O_3 + MoO_3$ (calculated, 4.1%) is followed by a second weight loss of 79.1%, which occurs over the range $700 \le T/°C \le 920$ as the result of volatalization of MoO_3 (calculated, 81.1%). Thermogravimetric data for the intermediate compositions, provided as Supporting Information, show three distinct weight changes due to, in order of increasing temperature, conversion to oxides, oxidation of V_4O_9 to V_2O_5, and volatilization of MoO_3. Initial conversion of materials containing both molybdenum and vanadium to a mixture of oxides requires higher temperatures than for either of the end-member phases. With decreasing molybdenum contents, deviation between the experimentally determined final weight loss and that calculated for complete volatalization of MoO_3 increases. This appears to be due to deposition of MoO_3 on the cooler parts of the thermobalance. For this reason only the initial oxidation was used to determine the sulfur contents shown in Table 1, where thermogravimetric data are summarized.

Magnetic susceptibility data are presented in Figure 5. For all materials, zero-field-cooled and field-cooled data overlie each other over the entire temperature range studied. The mixed $GaV_{4-x}Mo_xS_8$ ($1 \le x \le 3$) phases follow Curie−Weiss behavior over a wide temperature range, showing only slight curvature away from linearity in the reciprocal susceptibility plot at low temperatures (Figure 5), while the end-member phases show rather different behavior. Data for GaV_4S_8 are well described by a modified Curie−Weiss law, incorporating a temperature-independent term, down to 45 K. Below this temperature, there is a marked discontinuity in the reciprocal susceptibility plot at 40 K, and, on further cooling, a second discontinuity is observed at ca. 9 K: both temperatures being established through examination of $d(1/\chi)/dT$. Similarly, $GaMo_4S_8$ follows Curie−Weiss behavior down to 55 K. Below this temperature, the behavior is similar to that of GaV_4S_8, with anomalies occurring at 45 K and 19 K. Parameters derived from the linear fits to reciprocal susceptibility data are presented in Table 2. The effective magnetic moment of ca. $1.5\mu_B$ per V_4 cluster in GaV_4S_8 is close to that expected for a single unpaired electron as suggested by the molecular orbital treatment of Pocha et al.[11] With increasing substitution of vanadium by molybdenum, the moment increases and reaches a maximum at the composition $GaV_2Mo_2S_8$, before falling as the level of molybdenum incorporation rises toward that of the end-member, $GaMo_4S_8$. This behavior is consistent with the addition of one electron to t_2-type cluster orbitals for each unit increment in x: the number of unpaired electrons being a maximum (of 3) at $x = 2$. However, the magnitude of the moments in the V/Mo phases is markedly lower than would be expected for spin-only behavior, suggesting either that the moments are not fully localized or that there are magnetic exchange interactions within the cluster. The small negative Weiss constants, which suggest that intracluster interactions are antiferromagnetic, supports the latter view.

The field dependence of the magnetization of GaV_4S_8 at 5 K (Figure 6) reveals a spontaneous magnetization that approaches saturation in an applied field of 10 kG. By contrast, although the analogous data for $GaMo_4S_8$ also suggest a spontaneous magnetization, the moment is far from saturation even at 10 kG. Estimates of the saturated moment were obtained by taking the intercept on the moment axis of linear

(15) Garrett, R. F.; Cookson, D. J.; Foran, G. J.; Sabine, T. M.; Kennedy, B. J.; Wilkins, S. W. *Rev. Sci. Instrum.* **1995**, *66*, 1351.
(16) Larson, A. C.; von Dreele, R. B. *General Structure Analysis System*; Report LAUR 85-748; Los Alamos Laboratory: 1994.

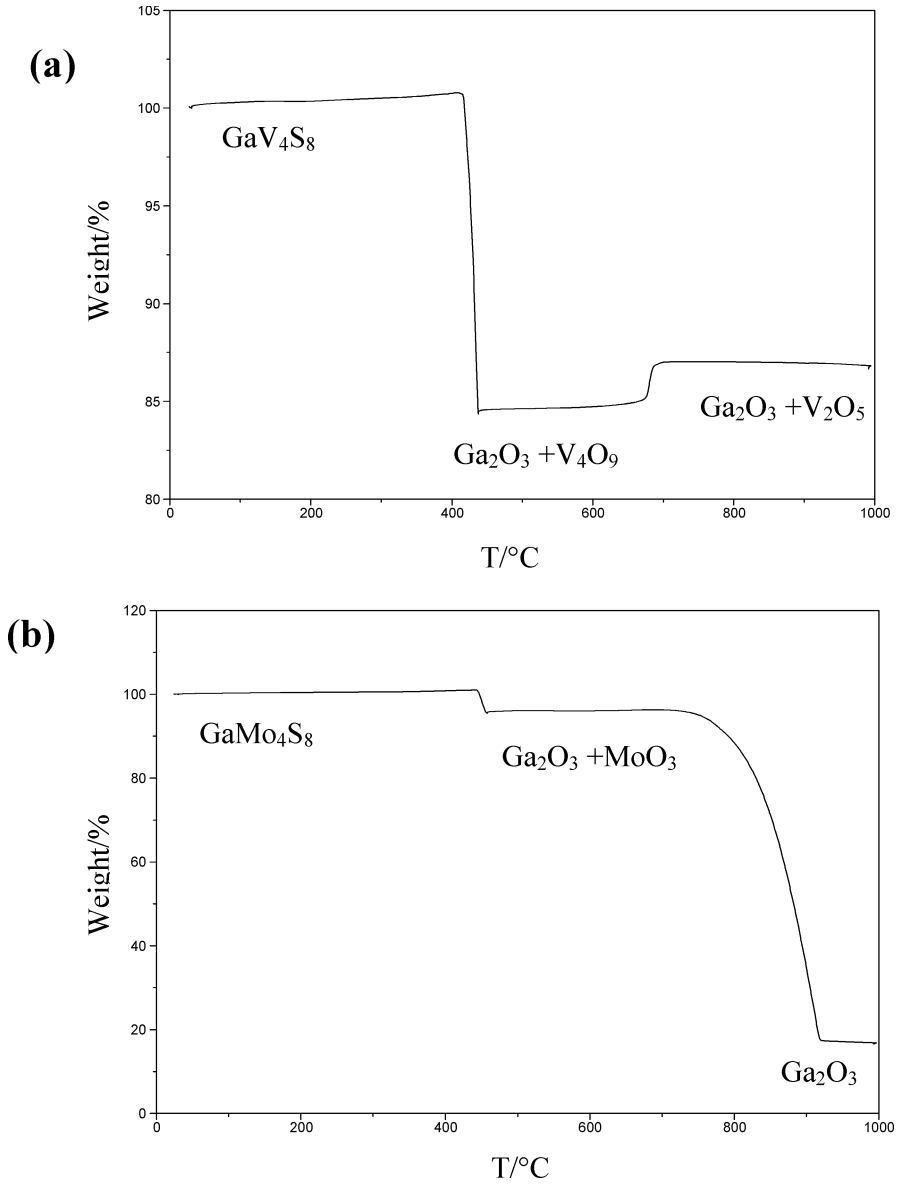

Figure 4. Thermogravimetric data for (a) GaV_4S_8 and (b) $GaMo_4S_8$.

Table 1. Results of Thermogravimetric Analysis for $GaV_{4-x}Mo_xS_8$ ($0 \le x \le 4$)

	x in $GaV_{4-x}Mo_xS_8$				
	0.0	1.0	2.0	3.0	4.0
T_1/°C	425	505	500	460	450
weight loss at T_1/%	15.58	12.27	9.17	6.05	4.14
weight gain at T_2/%	2.30	1.42	1.25	0.54	
weight loss at $T \ge 700$ °C		11.50	43.42	67.73	79.14
experimentally determined composition	$GaV_4S_{7.8}$	$GaV_3MoS_{7.8}$	$GaV_2Mo_2S_{7.7}$	$GaVMo_3S_{7.6}$	$GaMo_4S_{7.6}$

fits to the high-field region of μ vs $1/H$ plots, leading to values for GaV_4S_8 and $GaMo_4S_8$ of 0.778(2) and 0.85(1) μ_B per B_4 cluster respectively, both of which are slightly reduced from the value of 1.0 μ_B expected for a single unpaired electron.

Rietveld analyses of the data from $GaV_{4-x}Mo_xS_8$ phases at 300 K ($0 \le x \le 3$) and 150 K($x=4$) were initiated in the space group $F\bar{4}3m$, using for the initial structural model, the coordinates reported by Pocha et al.[11] for GaV_4S_8. Owing to the small neutron scattering length of vanadium, structural refinement of the end-member, $x = 0$, phase was performed using powder neutron and synchrotron X-ray diffraction data simultaneously. The peak shape in the neutron data was described by a convolution of an exponential and a pseudo-Voigt function and that in the X-ray data by a pseudo-Voigt function. In each case, the coefficients were included as refinable parameters. Regions centered at $d \approx 2.1$, 1.5, and 1.2 Å in the neutron data were excluded from the refinements owing to the presence of weak reflections arising from vanadium of instrumental origin.

In the substituted phases, molybdenum was introduced into the structural model at the vanadium (16(e)) site to maintain the correct stoichiometry. Refinement produced residuals in the range 2.5−3.0% (neutron) and 2.3−5.4% (X-ray). However, for the composition with $x = 1$, while the quality of the refinement using data from the 90° bank was

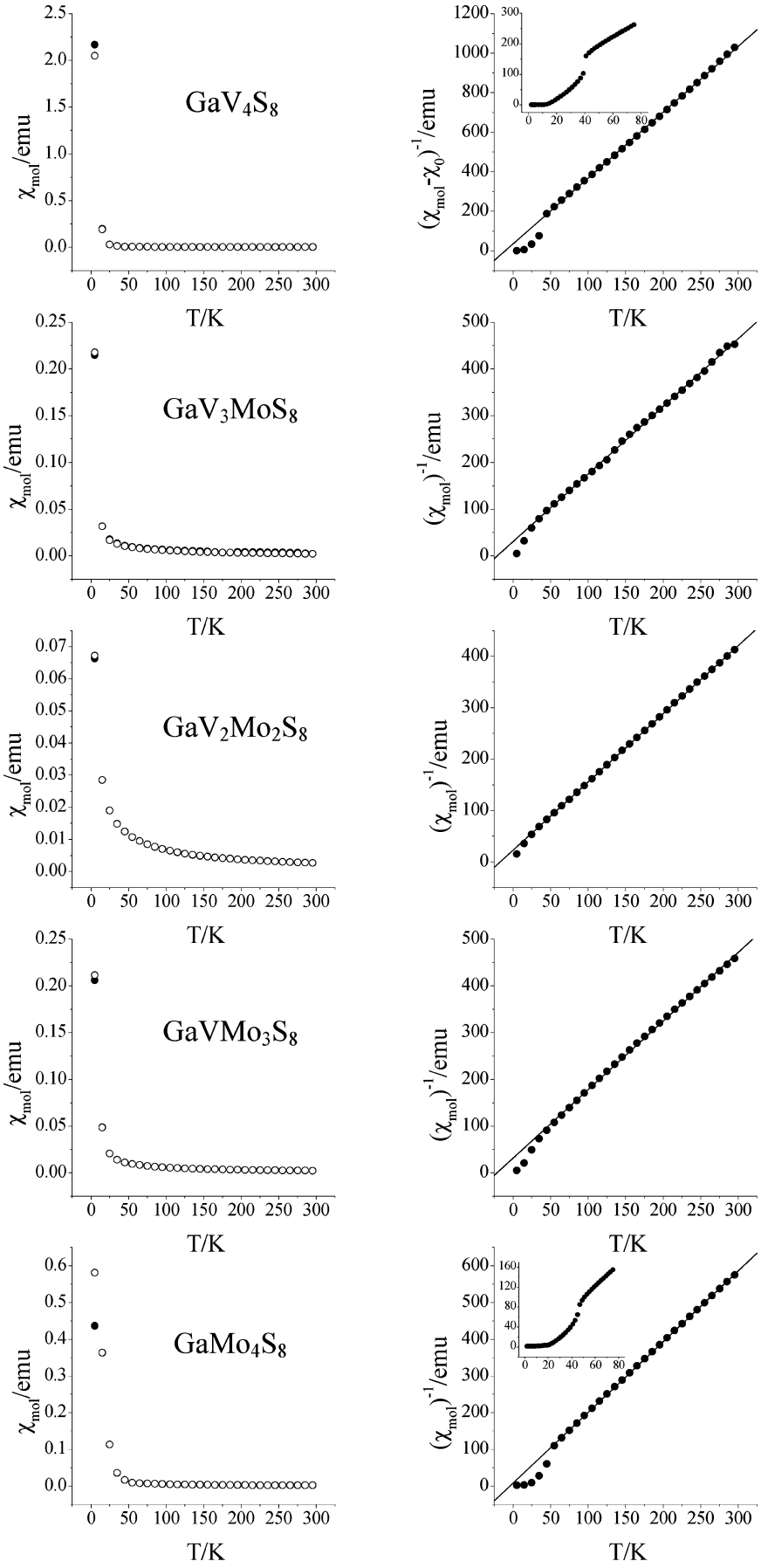

Figure 5. Magnetic data for $GaV_{4-x}Mo_xS_4$ ($0 \leq x \leq 4$). Left column: zero-field cooled (solid circles) and field-cooled (open circles) molar magnetic susceptibilities measured in a field of 1 kG. Right column: observed (points) and calculated (full line) reciprocal susceptibility data. The calculated line is derived from the fit to a Curie−Weiss ($1 \leq x \leq 4$) or modified Curie−Weiss law ($x = 0$). Insets show detail around the transitions for GaV_4S_8 and $GaMo_4S_8$.

Table 2. Magnetic Properties of $GaV_{4-x}Mo_xS_8$ ($0 \le x \le 4$) Phases Derived from Fits to a Curie−Weiss Expression

	fitting range/K	C/ $cm^3\ K\ mol^{-1}$	θ/K	μ_{eff} per B_4 cluster/μ_B
GaV_4S_8[a]	45−295	0.304(3)	−12.4(6)	1.559(8)
GaV_3MoS_8	35−295	0.690(4)	−20.7(7)	2.349(7)
$GaV_2Mo_2S_8$	25−295	0.831(5)	−23.6(9)	2.578(8)
$GaVMo_3S_8$	35−295	0.672(4)	−18.6(9)	2.318(7)
$GaMo_4S_8$	55−295	0.519(1)	−4.0(4)	2.037(3)

[a] Fit to a modified Curie−Weiss law incorporating a temperature-independent term, $\chi_0 = 4.3(1) \times 10^{-4}$ emu.

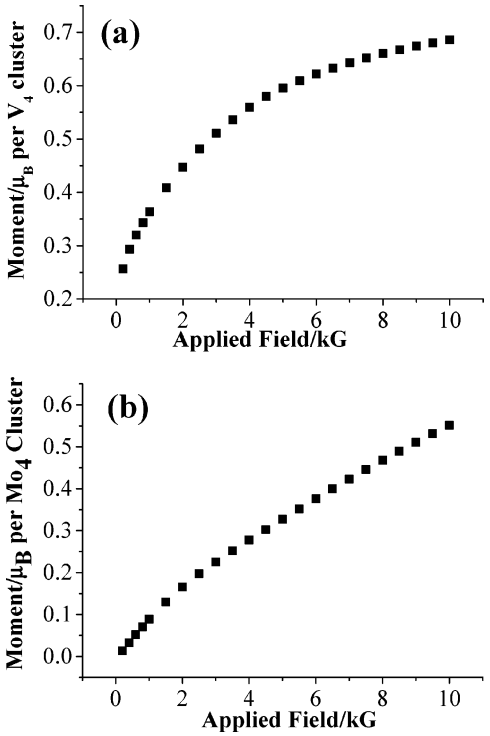

Figure 6. Variation in the magnetic moment per B_4 cluster of (a) GaV_4S_8 and (b) $GaMo_4S_8$ as a function of applied magnetic field at 5 K.

satisfactory, that using the high-resolution backscattering bank was significantly poorer (ca. 7.5%). Close examination of the reflections in these data suggested the presence of a second phase, indicated by a shoulder on the short *d*-spacing side of each of the peaks. Consequently, a second defect thiospinel phase with slightly different lattice parameters was introduced. Refinement of lattice parameters, atomic coordinates, and site occupancy factors confirms that at this composition phase separation has occurred to produce a majority phase ($GaV_{2.61(2)}Mo_{1.39(2)}S_8$) with a vanadium content lower than the nominal value and a minority phase ($GaV_{3.76(2)}Mo_{0.24(2)}S_8$) with an increased vanadium content. The stoichiometry and weight fractions of the two phases are consistent with phase separation occurring as follows:

$$GaV_3MoS_8 \rightarrow 0.66GaV_{2.61}Mo_{1.39}S_8 + 0.34GaV_{3.76}Mo_{0.24}S_8$$

Final observed, calculated, and difference X-ray and neutron profiles for refinements of GaV_4S_8 are given in Figure 7. Structural refinements for the cubic structure of the remaining compositions are of similar quality, and final observed, calculated, and difference profiles are provided as Supporting Information. The final refined parameters for all compositions are presented in Table 3, while selected bond lengths and angles appear in Table 4. Synchrotron X-ray data collected for GaV_4S_8 at higher temperatures reveal that the cubic structure persists to the highest temperature studied (473 K).

Rietveld analysis of data collected at lower temperatures was carried out in an analogous fashion to that described above. Data for the end-member phases GaV_4S_8 and $GaMo_4S_8$ are well-described by a cubic structure down to temperatures of 45 K and 50 K, respectively. However, this structural model does not provide an adequate description of the experimental neutron diffraction data collected at 30 K and below. The rhombohedral distortion expected on the basis of previous powder X-ray diffraction studies[11,13] is clearly identified in the high-resolution backscattering bank of HRPD by the splitting of the cubic (440) reflection that occurs at ca. 1.70 Å (Figure 8). However, these high-resolution data demonstrate that the phase transformation is incomplete and that both rhombohedral and cubic phases coexist at low temperatures. This coexistence demonstrates the transition between these two phases to be first-order. Therefore data for $x = 0$ and $x = 4$ were fitted using a two-phase model incorporating both cubic ($F\bar{4}3m$) and rhombohedral ($R3m$) structures. The coordinates reported by Francois et al.[13] for $GaMo_4S_8$ were used for the initial structural model in $R3m$ of both ternary phases. Refined weight fractions reveal that at 4.2 K ca. 40% by weight of $GaMo_4S_8$ consists of the cubic phase, while in the vanadium analogue the weight fraction of the cubic phase is ca. 7%. These proportions are affected slightly by the cooling rate and the data collection temperature. Final observed calculated and difference profiles for GaV_4S_8 and $GaMo_4S_8$ at 4.2 K appear in Figures 8 and 9, respectively. Refined parameters are shown in Table 5, and selected bond lengths and angles are presented in Table 6.

By contrast to the behavior of the end-member phases ($x = 0$, 4), the powder neutron diffraction data for the materials $GaV_{4-x}Mo_xS_8$ ($1 \le x \le 3$) are well-fitted by a cubic ($F\bar{4}3m$) structural model to the lowest temperatures studied. Final observed, calculated, and difference profiles for $GaV_2Mo_2S_8$ at 4.2 K are presented in Figure 10, while those for the remainder of the mixed vanadium−molybdenum-containing phases are provided as Supporting Information, together with refined parameters and significant distances and angles.

The distortion from cubic symmetry in the end-member phases is characterized by a marked discontinuity in the temperature variation of the unit cell parameters (Figure 11). The phase transition corresponds to a distortion of the B_4 cluster, the extent of which may be quantified through the parameter, *t*, defined by the following expression

$$t = \frac{1}{6}\sum_{i=1}^{6}|\langle d\rangle - d_i|$$

where $\langle d\rangle$ and d_i are the mean and individual metal−metal distances, respectively, and the summation is over all bonds in the cluster. Although the degree of distortion, *t*, is ca. 4% at 4.2 K in both GaV_4S_8 and $GaMo_4S_8$, the distortion of the cluster is in the opposing sense in the two cases. In the rhombohedral phase of $GaMo_4S_8$, contraction along a 3-fold

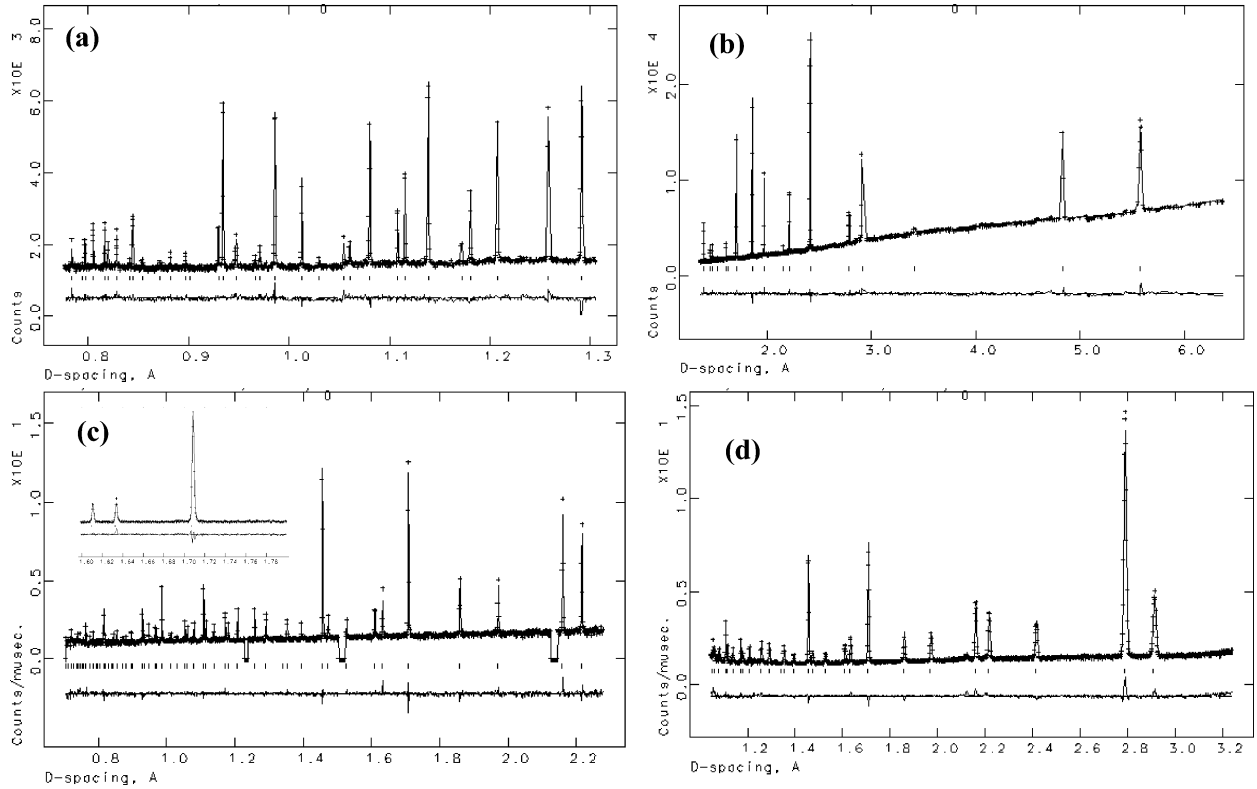

Figure 7. Final observed (crosses), calculated (upper full line), and difference (lower full line) profiles for GaV_4S_8 at 300 K: (a) and (b) synchrotron X-ray data from the two image plates, (c) neutron data from the backscattering detector bank with the cubic (440) reflection shown as an inset, and (d) neutron data from the 90° detector bank. Reflection positions are marked. Regions containing V peaks have been excluded.

Table 3. Final Refined Parameters for $GaV_{4-x}Mo_xS_8$ ($0 \le x \le 4$) Phases Described in the Space Group $F\bar{4}3m$[a]

		x in $GaV_{4-x}Mo_xS_8$				
		0	1[b]	2	3	4
	T/K	300	300	300	300	150
	a/Å	9.66302(2)	9.69145(6)	9.70963(4)	9.73191(2)	9.7272(1)
Ga	B/Å^2	0.51(2)	1.19(3)	1.11(6)	1.24(4)	0.21(1)
B	SOF(V)	1	0.652(4)	0.466(3)	0.21(-)	0
	SOF(Mo)	0	0.348(4)	0.534(3)	0.79(-)	1
	x	0.60563(5)	0.6008(2)	0.60116(9)	0.60329(6)	0.60296(6)
	B/Å^2	0.25(1)	0.74(9)	0.64(6)	0.46(2)	0.296(9)
S(1)	x	0.3720(1)	0.3690(2)	0.3675(2)	0.3681(2)	0.3646(2)
	B/Å^2	0.24(1)	1.19(4)	1.40(7)	0.49(6)	0.26(4)
S(2)	x	0.8635(1)	0.8639(2)	0.8648(2)	0.8623(1)	0.8647(2)
	B/Å^2	0.24(1)	1.15(4)	1.23(8)	0.49(6)	0.30(4)
R_{wp}/% (neutron)	(2θ=168°)	2.58	4.74	4.60	4.52	5.71
	(2θ=90°)	3.02	2.55	3.11	3.80	3.32
R_{wp}/% X-ray		5.40				
		2.30				

[a] Ga on 4(a): (0,0,0); B, S(1) and S(2) on 16(e): (x,x,x). [b] Parameters are given for the majority phase (weight fraction 61%).

Table 4. Bond Lengths (Å) and Angles (deg) for the High-Temperature Cubic Form of $GaV_{4-x}Mo_xS_8$

	x in $GaV_{4-x}Mo_xS_8$				
	0	1[a]	2	3	4
Ga−S(2)	4 × 2.292(2)	4 × 2.284(4)	4 × 2.274(3)	4 × 2.321(2)	4 × 2.280(3)
B−S(1)	3 × 2.273(1)	3 × 2.285(3)	3 × 2.309(2)	3 × 2.323(2)	3 × 2.361(2)
B−S(2)	3 × 2.519(1)	3 × 2.596(3)	3 × 2.602(2)	3 × 2.565(1)	3 × 2.584(2)
B−B	6 × 2.898(2)	6 × 2.763(6)	6 × 2.778(3)	6 × 2.843(2)	6 × 2.832(2)
S(2)−Ga−S(2)	6 × 109.471(-)	6 × 109.471(-)	6 × 109.471(-)	6 × 109.471(-)	6 × 109.471(-)
S(1)−B−S(1)	3 × 99.86(5)	3 × 103.6(1)	3 × 103.97(8)	3 × 102.82(7)	3 × 104.16(6)
S(1)−B−S(2)	6 × 91.02(4)	6 × 89.2(1)	6 × 88.77(8)	6 × 89.72(7)	6 × 88.38(7)
S(2)−B−S(2)	3 × 75.65(6)	3 × 74.0(1)	3 × 74.57(9)	3 × 74.12(7)	3 × 75.23(9)

[a] Parameters are given for the majority phase (weight fraction 61%).

axis of the cubic unit cell expands the Mo(1)−Mo(2)−Mo(1) angle within the cluster from 60° to 61.6(3)°, whereas in the vanadium analogue, expansion along the same axis results in a contraction of this angle to 58.3(7)°. This opposing behavior has been rationalized by Pocha et al.,[11] by consideration of the different orbital occupancies of the cluster-based orbitals (Figure 2). In both $GaMo_4S_8$ and GaV_4S_8, the distortion removes the orbital degeneracy

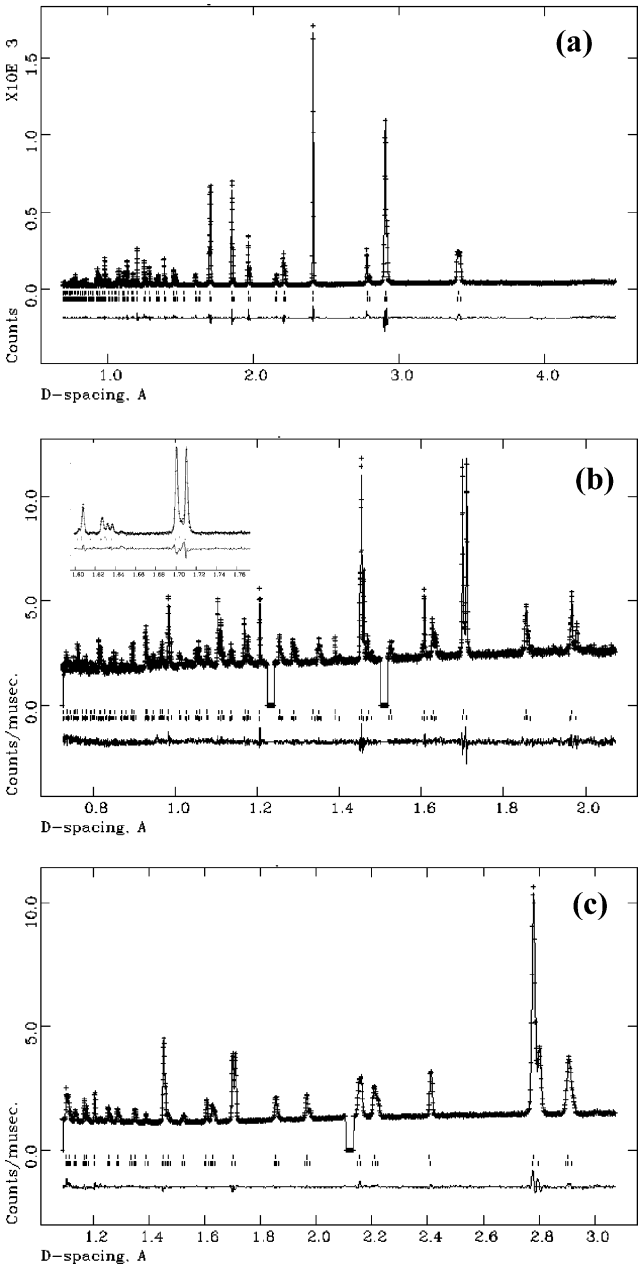

Figure 8. Final observed (crosses), calculated (upper full line), and difference (lower full line) profiles for GaV_4S_8 at low temperatures: (a) synchrotron X-ray diffraction data at 20 K, (b) neutron diffraction data at 4.2 K from the backscattering detector bank, the inset showing the rhombohedral splitting of the cubic (440) reflection and the coexistence of cubic and rhombohedral phases, and (c) neutron diffraction data at 4.2 K from the 90° detector bank. In each case, the upper set of reflection markers refers to the cubic phase, and the lower set refers to the rhombohedral phase.

associated with the t_2 HOMO, stabilizing an a_1 orbital for a decreased rhombohedral angle and destabilizing it for an increased angle. The former leads to a lowering of energy for the t_2^1 configuration in GaV_4S_8, whereas the latter is energetically favored for t_2^5 in the molybdenum analogue. On electronic grounds therefore it would be anticipated that mixed $GaV_{4-x}Mo_xS_8$ ($1 \leq x \leq 3$) phases would exhibit a rhombohedral distortion involving an expansion of the intracluster angle for $x = 1$ (t_2^2) and a contraction for $x = 3$ (t_2^4): the expectation being that the nondegenerate t_2^3 ground state of the phase with $x = 2$ would remain cubic. However, the data presented here for phases in which the HOMO electron count is systematically varied reveal that the phases

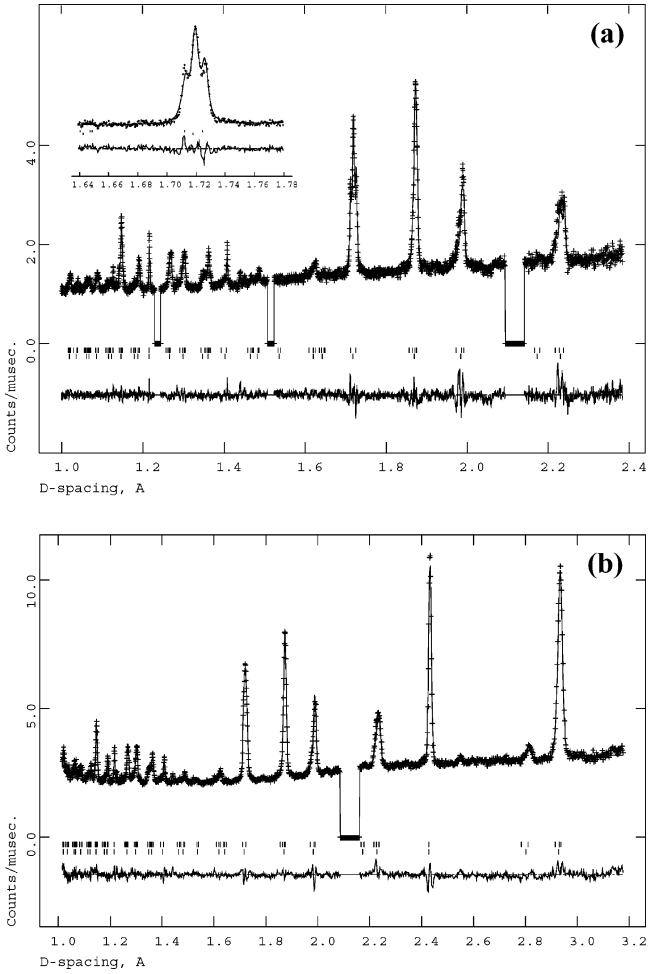

Figure 9. Final observed (crosses), calculated (upper full line), and difference (lower full line) neutron diffraction profiles for $GaMo_4S_8$ at 4.2 K: (a) data from the backscattering detector bank. (The inset showing the rhombohedral splitting of the cubic (440) reflection clearly demonstrates that a greater proportion of the cubic phase persists to low temperatures than is the case with GaV_4S_8. (b) Data from the 90° detector bank. In each case, the upper set of reflection markers refers to the cubic phase, and the lower set refers to the rhombohedral phase.

in the composition range $1 \leq x \leq 3$ remain cubic to 4.2 K, suggesting that the appearance of a low-temperature distortion may not be a consequence of electronic factors alone. The persistence of a cubic structure in the molybdenum-substituted phases indicate that disorder on the cation sites, which leads to mixed $(V,Mo)_4$ clusters of varying composition, may play a role in lifting the degeneracy at a local level within the cluster.

In the present work, we have demonstrated that in both $GaMo_4S_8$ and GaV_4S_8, the phase transition is incomplete. This coexistence of both cubic and rhombohedral phases at low temperatures may be responsible for the difficulties reported elsewhere[11] in obtaining high-quality structural refinements from powder diffraction data, where the resolution was insufficient to resolve the distortion. The weight fractions of the two phases at 4.2 K show only a slight dependence on the rate of cooling of the sample. For example, for $GaMo_4S_8$, the weight fraction of the cubic phase at 4.2 K varies from ca. 41.2% for a sample cooled at 20 Kh^{-1} to ca. 50% when cooled rapidly (ca. 120 Kh^{-1}). This suggests that the phase separation is not due to straightforward thermal quenching of the high-temperature phase but

Table 5. Final Refined Parameters for the Low-Temperature Rhombohedral Phase of $GaV_{4-x}Mo_xS_8$ ($x = 0, 4$) Phases Described in the Space Group *R*3*m*[a]

	x	0	0	4
	T/K	4.2	20	4.2
	wt fraction/%	92.84(1)	85.2(1)	58.8(5)
	a/Å	6.83974(4)	6.83870(4)	6.8527(2)
	α/°	59.616(1)	59.643(1)	60.468(2)
Ga	B/Å^2	0.46(3)	0.09(1)	0.46(9)
	x	0(-)[b]	0(-)[b]	0(-)[b]
B(1)	B/Å^2	0.46(3)	0.09(1)	0.46(9)
	x	0.391(2)	0.3901(2)	0.4014(7)
B(2)	B/Å^2	0.46(3)	0.09(1)	0.46(9)
	x	0.395(2)	0.3952(2)	0.3979(8)
	z	0.814(3)	0.8152(3)	0.811(1)
S(1)	B/Å^2	0.56(2)	0.14(1)	0.19(9)
	x	0.6298(3)	0.6302(3)	0.636(1)
S(2)	B/Å^2	0.56(2)	0.14(1)	0.19(9)
	x	0.6253(4)	0.6282(3)	0.647(2)
	z	0.1129(6)	0.1103(5)	0.085(2)
S(3)	B/Å^2	0.56(2)	0.14(1)	0.19(9)
	x	0.1353(3)	0.1350(3)	0.132(2)
S(4)	B/Å^2	0.56(2)	0.14(1)	0.19(9)
	x	0.1336(3)	0.1323(3)	0.132(1)
	z	0.5895(6)	0.5967(5)	0.596(2)
R_{wp}/% (neutron)	(2θ=168°)	3.71		4.74
	(2θ=90°)	2.34		3.62
R_{wp}/% X-ray			6.28	

[a] Ga, B(1), S(1), and S(3) on 1(a): (x,x,x); B(2), S(2), and S(4) on 3(b): (x,x,z). [b] Fixed to define the origin.

Table 6. Significant Bond Lengths (Å) and Angles (deg) for the Low-Temperature Rhombohedral Form of $GaV_{4-x}Mo_xS_8$ ($x = 0, 4$)

	$x = 0$ (4 K, neutron)	$x = 0$ (20 K, X-ray)	$x = 4$
Ga−S(3)	2.273(5)	2.267(5)	2.202(27)
Ga−S(4)	3 × 2.282(3)	3 × 2.242(3)	3 × 2.274(12)
B(1)−S(2)	3 × 2.278(13)	3 × 2.312(3)	3 × 2.440(15)
B(1)−S(4)	3 × 2.518(19)	3 × 2.513(3)	3 × 2.666(16)
B(2)−S(1)	2.293(21)	2.294(4)	2.357(18)
B(2)−S(2)	2 × 2.292(15)	2 × 2.300(3)	3 × 2.376(13)
B(2)−S(3)	2.538(18)	2.540(3)	2.620(13)
B(2)−S(4)	2.517(15)	2 × 2.532(2)	2 × 2.562(11)
B(1)−B(2)	3 × 2.920(26)	3 × 2.943(3)	3 × 2.780(10)
B(2)−B(2)	3 × 2.846(26)	3 × 2.856(3)	3 × 2.848(9)
S(3)−Ga−S(4)	3 × 110.58(9)	3 × 110.26(8)	3 × 110.1(4)
S(4)−Ga−S(4)	3 × 108.34(9)	3 × 108.68(8)	3 × 108.8(4)
S(2)−B(1)−S(2)	3 × 99.8(8)	3 × 99.2(1)	3 × 105.2(3)
S(2)−B(1)−S(4)	6 × 90.9(2)	6 × 90.47(8)	6 × 88.2(4)
S(4)−B(1)−S(4)	3 × 76.0(7)	3 × 77.9(1)	3 × 73.8(5)
S(1)−B(2)−S(2)	2 × 102.1(5)	2 × 101.93(7)	2 × 103.23(33)
S(1)−B(2)−S(4)	2 × 90.2(7)	2 × 89.7(1)	2 × 89.5(5)
S(2)−B(2)−S(2)	98.9(9)	99.9(2)	109.3(8)
S(2)−B(2)−S(3)	2 × 89.6(6)	2 × 89.38(9)	2 × 87.5(5)
S(2)−B(2)−S(4)	2 × 90.9(2)	2 × 90.0(1)	2 × 84.7(4)
S(3)−B(2)−S(4)	2 × 75.5(4)	2 × 76.49(9)	2 × 75.8(4)
S(4)−B(2)−S(4)	76.0(5)	77.2(1)	77.4(6)

is an intrinsic feature of the system, which may be the result of strain or of defects. Examination of the peak shape provides support for the suggestion that strain has an influence on the phase transition. A high-quality structural refinement of GaV_4S_8 at 4.2 K, which consists of over 90% of the rhombohedral phase, was obtained by using a convolution of a pseudo-Voigt function with two exponentials to model the peak shape. However, application of this peak-shape function to the analysis of the analogous data for $GaMo_4S_8$ resulted in significant features remaining in the difference profile and convergence of the refinement with $\chi^2 = 7.6$. Close examination of the profiles suggested that anisotropic line broadening was the major factor in those

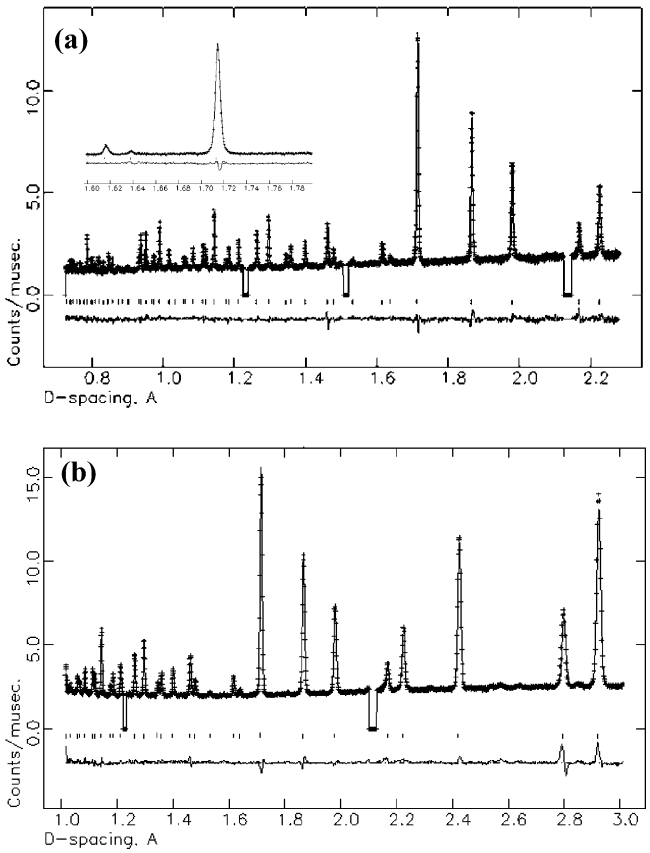

Figure 10. Final observed (crosses), calculated (upper full line), and difference (lower full line) powder neutron diffraction profiles for $GaV_2Mo_2S_8$ at 4.2 K: (a) neutron data from the backscattering detector bank, with the cubic (440) reflection shown as an inset, and (b) neutron data from the 90° detector bank. Reflection positions are marked.

regions where the fit was unsatisfactory. It was therefore necessary to introduce into the refinement terms to account for strain-induced displacement and anisotropic microstrain peak broadening. This modified peak shape produced a significant improvement in the quality of fit, with χ^2 falling to 2.6. A demonstration of the improvement in the quality of fit obtained through the incorporation of terms to account for strain is provided in the Supporting Information (Figure S4).

The data presented here indicate that magnetic order in the defect thiospinels is intimately linked to the occurrence or absence of a structural distortion. This conclusion is further supported by the recent work of Müller et al.,[12] who have demonstrated by powder neutron diffraction that the low-temperature antiferromagnetically ordered state of GeV_4S_8 is associated with a distortion to an orthorhombic structure. In the magnetically ordered state, moments within the cluster are ferromagnetically coupled, and adjacent clusters in the [010] direction are antiferromagnetically aligned. Furthermore neutron measurements, supported by calculations, reveal that the spin density is effectively localized on one (2-fold) site of the cluster.

In contrast to GeV_4S_8, magnetic susceptibility data for GaV_4S_8 and $GaMo_4S_8$ clearly indicate the appearance at low temperatures of a spontaneous magnetization. Although no magnetic scattering was detectable in our low-temperature neutron diffraction measurements, calculations[12] on the

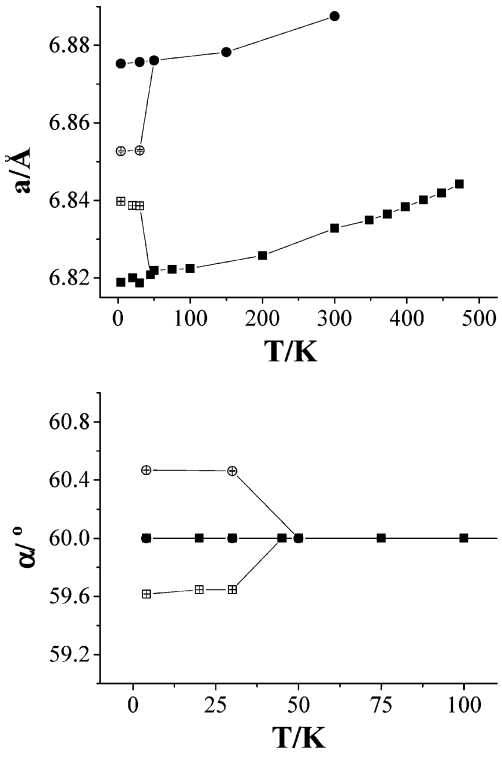

Figure 11. The temperature dependence of the unit cell parameters, a and α, of GaV_4S_8 (circles) and $GaMo_4S_8$ (squares). To aid comparison, lattice parameters for the cubic structure have been converted to the rhombohedral unit cell of the low-temperature phase through $a_R = a_c/\sqrt{2}$ and $\alpha_R = 60°$. Solid points refer to the cubic structure, while open points refer to the rhombohedrally distorted structure. The solid lines are a guide to the eye. In some instances, error bars lie within the points.

ferromagnetic ground state of rhombohedral GaV_4S_8 also reveal spin localization, with the majority of unpaired spin residing on the apical vanadium ion of the V_4S_4 cluster. A calculated value of 0.696 spins associated with this ion suggests that moments are likely to be small, which may account for the absence of any detectable magnetic scattering. The negative Weiss constants indicate that the dominant magnetic interactions are antiferromagnetic in origin, suggesting that the spontaneous magnetization may arise from incomplete cancellation of the antiferromagnetically coupled moments of the four atoms of the cluster. In the ideal cubic structure, the four transition-metal cations adopt a tetrahedral arrangement. This topology does not permit all nearest-neighbor antiferromagnetic interactions to be satisfied simultaneously, and the system would therefore be geometrically frustrated.[17] The distortion on cooling below 40 K ($x = 0$) or 45 K ($x = 4$) results in the six equivalent cation−cation distances of the cubic phase becoming inequivalent. The presence of three longer and three shorter cation−cation distances as a result of the structural distortion may provide a mechanism for relieving the nearest neighbor frustration, leading to magnetic order in the rhombohedrally distorted phase.

Acknowledgment. We wish to thank the U.K. EPSRC for the provision of a studentship for A.D.M. and for a grant in support of our neutron scattering program. The ASRP supported the synchrotron studies at the Photon Factory.

Supporting Information Available: Additional thermogravimetric data and final observed, calculated, and difference profiles from Rietveld analysis of powder diffraction data. This material is available free of charge via the Internet at http://pubs.acs.org.

CM071354T

(17) Greedan, J. E. *J. Mater. Chem.* **2001**, *11*, 37.